Available at www.sciencedirect.com

ScienceDirect

journal homepage: www.elsevier.com/locate/issn/15375110

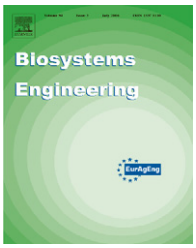

Research Paper: AE—Automation and Emerging Technologies

Water stress detection in Sunagoke moss (*Rhacomitrium canescens*) using combined thermal infrared and visible light imaging techniques

S. Ondimu, H. Murase*

Bio-instrumentation, Control and Systems (BICS) Engineering Laboratory, College of Life and Environmental Sciences, Osaka Prefecture University, 1-1, Gakuen-cho, Sakai, Japan

ARTICLE INFO

Article history:
Received 16 November 2006
Received in revised form
10 December 2007
Accepted 8 February 2008
Available online 20 March 2008

This study is a contribution to an ongoing research to develop a thermal-reflectance imaging system (TRIS) for detecting water stress in Sunagoke moss (*Rhacomitrium canescens*). The correlation between visual and thermal water stress symptoms in a sample of Sunagoke moss as a function of time and water content was evaluated. Visible light imaging was used to report changes in the surface structure and reflectance. Infrared (IR) thermal imaging was used to monitor transpiration patterns and the crop water stress index (CWSI) was used to quantify those changes. Grey-level concurrence matrix (GLCM) texture features were used to quantify changes in the sample surface structure while the RGB colour ratios were used to detect changes in its reflectance. The sample exhibited water-related stress at water contents below 1.5 $g\,g^{-1}$ and above 3.0 $g\,g^{-1}$ (grams of water per gram of dry sample). The maximum possible total uncertainty of IR temperatures for the sample was $\pm 0.50\,^{\circ}C$ at 17 °C, ambient temperature. The maximum uncertainty of its visible light data was ± 7.65 grey level attributed to the red bandwidth. The results showed a clear correlation between the water status of the sample and its CWSI, GLCM texture and RGB colour ratios. These results demonstrate the possibility of detecting both drought and flood water stress in Sunagoke moss by combining thermal and visible light imaging. Although Sunagoke moss was used in this study, this method is novel and could be extended to both biotic and abiotic stress detection in other plants.

1. Introduction

Plant stress is defined as an external factor that exerts a disadvantageous influence on plants (Taiz and Zeiger, 2002). Plant water stress is caused by water deficit or excess. The response of a plant to water stress is expressed at genetic (DNA), cellular, organ and whole plant levels. This is reflected in its surface structure and transpiration patterns as the top projected canopy area (TPCA) and canopy temperature or multispectral reflectance. Imaging techniques can monitor changes in water status, photosynthetic efficiency, accumulation of secondary metabolites or structural modifications. This makes the real-time analysis of physiological changes in plants, often characterised by numerous dynamics and non-linearity (Hall and Lima, 2001), possible. Imaging techniques that have been used to detect signs of stress in plants include fluorescence, bioluminescence, thermal, magnetic resonance and reflectance imaging (Chaerle and Van Der Straeten, 2001).

*Corresponding author. Tel.: +81 72 254 9429.
E-mail address: ondimu@bics.envi.osakafu-u.ac.jp (S. Ondimu).
1537-5110/$ - see front matter © 2008 IAgrE. Published by Elsevier Ltd. All rights reserved.
doi:10.1016/j.biosystemseng.2008.02.005

Nomenclature

a	intercept of a linear fit of the ratio between determined standard deviation and the expected standard deviation (were the errors to follow a normal distribution)
b	Wein's displacement constant ($2.8977685 \pm 5.1 \times 10^{-9}$ W K)
c	speed of light in m s^{-1}
dT	plant surface-ambient temperature difference, °C
dT_l	plant surface-ambient temperature difference of a well-watered plant (lower limit), °C
dT_u	plant surface-ambient temperature difference of a non-transpiring plant (upper limit), °C
E	radiation energy, J
e_{ref}	emissivity of the reference emitter
e_{ms}	emissivity of the Sunagoke moss sample
m	slope of a linear fit of the ratio between the determined standard deviation and the expected standard deviation (were the errors to follow a normal distribution)
h	Plank's constant (6.69×10^{-34} J Hz^{-1})
N	number of temperature data points evaluated
n	number of hours over which thermographic frames are averaged
q	radiation energy, W m^{-2} K^{-4}
T	obsolute temperature of a black body, K
$T_{DC,ref}$	direct contact temperature of the reference emitter, °C
$T_{e=1,ms}$	equivalent black body infrared temperature of the Sunagoke moss sample, °C
$T_{e=1,ref}$	equivalent black body infrared temperature of the reference emitter, °C
$T_{F,ms}$	final infrared temperature of the Sunagoke moss sample, °C
$T_{IR,ms}$	apparent infrared temperature of the Sunagoke moss sample, °C
$T_{IR,ref}$	apparent infrared temperature of the reference emitter, °C
T_m	spatial mean of the measured temperature, °C
T_p	temperature data points, °C
v	frequency, Hz
α	absorptivity
δT	maximum total uncertainty, °C
$\delta T_{DC,A}$	uncertainty of direct contact ambient temperature, °C
$\delta T_{DC,ref}$	uncertainty of the reference emitter's direct contact temperature, °C
$\delta T_{F,ms}$	uncertainty of Sunagoke moss sample thermographic data, °C
$\delta T_{IR,FOV}$	uncertainty resulting from the thermal imager's field of view, °C
$\delta T_{IR,ms}$	uncertainty of the apparent infrared temperature of the Sunagoke moss sample, °C
$\delta T_{IR,ref}$	uncertainty of the apparent infrared temperature of the reference emitter, °C
$\delta T_{p,ran}$	random error, °C
ε	emissivity
λ	radiation wavelength, m
λ_{max}	peak wavelength, m
σ_p	standard deviation of temperature data points, °C
σT_{FOV}	standard deviation of thermographic data in the thermal imager's field of view, °C

A combination of infrared (IR) thermal and visible light imaging for detecting water-related stress in Sunagoke (*Rhacomitrium canescens*) moss is reported in this paper.

Many studies have reported the use of IR thermography and visible light imaging to detect stress in plants. Hashimoto et al. (1984) used thermal imaging to show that water stress in sunflower plants first develops at leaf margins, accompanied by stomatal closure and an increase in leaf surface temperature. Zandonadi et al. (2005) achieved an 81.6% efficiency in identifying maize attacked by lesser cornstalk borer using IR imaging. Al-Fara et al. (2000) used IR to obtain the canopy temperature, irradiance and vapour pressure of tall fescue (*Festuca arundinacea*) as inputs to Laplace transform models to illustrate the complex nature of plant feedback mechanisms when anticipating moisture stress. In another study, Wanjura and Upchurch (2000) showed that the theoretical crop water stress index (CWSI-T) was more accurate than an empirical canopy temperature water stress index (CWSI-TC) in characterising deficit water stress in corn (maize) and cotton. Kacira et al. (2002a) suggested the feasibility of using IR thermometry for pre-visual and non-contact detection of plant water stress. Other researches (Clarke, 1997; Jensen et al., 1990; Jackson, 1982; Pieters, 1975) also reported the use of plant surface temperature to quantify water stress in plants. Foucher et al. (2004) reported use of morphological features obtained by visible light imaging to detect water stress in potted forsythia. An investigation by Sena et al. (2003) achieved 94.72% efficiency in classifying army worm damage in maize using visible light imaging. In another study, Kacira et al. (2002b) showed that TPCA extracted from plant images can be used to quantify water stress.

These studies show that plant water status can be detected by thermal and visible light imaging. However, no study has reported the use of either of these techniques for stress detection in Sunagoke moss. In addition, although mainly deficit water stress has been highlighted so far, stress in plants can also be caused by excess water. In this paper IR thermal and visible light imaging were used to detect water stress in Sunagoke moss (Class: *Musci* and Division: *Bryophyta*). This plant is being investigated as a possible bio-roof and bio-wall "greening" material for urban heat island mitigation (Ondimu and Murase, 2006; Ushada and Murase, 2006). The plant has many unique qualities: it is resilient with minimum maintenance, is not susceptible to pests and diseases, requires no soil growing media, and retains its dark green colour even at temperatures as low as −30 °C or as high as 40 °C. In addition, it has a high level of desiccation tolerance (Aro et al., 1981; Bowen, 1933; Valanne, 1984) because it suspends its photosynthesis and transpiration when dry only to resume biological activity when later exposed to moisture.

However, optimum rates of net fixation are achieved only at certain water states, below which it is incapable of photosynthesis and above which photosynthetic activity declines. Thus, water stress is the main factor limiting its production.

This paper is a contribution towards an ongoing research to develop a thermal-reflectance imaging system (TRIS) for water stress diagnosis and monitoring in a Sunagoke moss production system. The investigation is based on the assumption that changes in surface structure, reflectance and transpiration patterns are expressions of internal physiological changes in plants. We hypothesise that simultaneous changes in colour, texture and temperature in Sunagoke moss canopy are direct indicators of its physiological stress state. The main objective of this study was to use thermal and visible light image analysis to evaluate the correlation between visual and thermal water stress symptoms in Sunagoke moss as a function of time. The study involved: (1) the evaluation of the crop water stress index (CWSI) using IR-measured surface temperatures, (2) evaluation of grey-level co-occurrence matrix (GLCM) textural features and RGB colour ratios of Sunagoke moss sample images and (3) evaluation of the correlation between CWSI values, texture and RGB colour ratios of the sample at different water states.

2. Materials and methods

2.1. Basic theory

2.1.1. Thermal imaging

Modifications in the water status of a plant caused by adverse conditions lead to changes in leaf transpiration due to the active regulation of the stomatal aperture. The associated changes in leaf cooling patterns can be monitored instantly and non-destructively by IR thermal imaging. Since, in general, metabolism has a negligible influence on plant temperature (Chaerle and Van Der Straeten, 2001) IR thermography can be used for stress detection in plants.

Thermal imaging is a non-invasive technique for measuring surface temperatures by observing IR radiation emitted from the surface. IR radiation impacting on a given surface is absorbed, reflected or transmitted. Of the absorbed radiation a proportion is re-emitted and another part is reflected internally. At thermal equilibrium bodies emit all the absorbed energy as described by Kirchoff's law of emission:

$$\alpha = \varepsilon \tag{1}$$

where α and ε are the absorptivity and emissivity at a given wavelength, respectively. The relationship between radiation energy, temperature and spectral emissivity is given by Plank's law:

$$E = h\upsilon \tag{2}$$

where E is the radiation energy in joules (J), h is Planks constant and υ is the frequency in Hz given by c/λ (c is the speed of light in $m\,s^{-1}$ and λ is the radiation wavelength in m). The wavelength at which maximum emission occurs is given by Wein's displacement law:

$$\lambda_{max} = \frac{b}{T} \tag{3}$$

where λ_{max} is the peak wavelength in metres (m), T is the absolute temperature of a blackbody in Kelvin (K) and b is Wien's displacement constant. Eqs. (1)–(3) are combined in the Stephan–Boltzmann Law:

$$q = \delta T^4 \tag{4}$$

where q is the radiation energy flux in $W\,m^{-2}$, δ is the Stefan–Boltzmann constant and T is the absolute temperature of a black body in K. Eqs. (1)–(4) apply for black bodies and should include emissivity (ε) for real surfaces. The IR sensor used in this study used Eq. (4) to compute the temperature of the Sunagoke moss sample. Values of CWSI, determined by Eq. (5), were used to relate surface temperature to water stress in the plant (González-Dugo et al., 2006; Jackson, 1982; Jackson et al., 1981).

$$CWSI = \frac{dT - dT_l}{dT_u - dT_l} \tag{5}$$

where dT is the measured plant surface–air temperature difference, dT_u is the plant surface–air temperature difference of a non-transpiring plant (upper limit) and dT_l is the plant surface–air temperature difference of a well-watered plant (lower limit).

2.1.2. Visible reflectance imaging

Stress in plants induces changes on the surface and the internal leaf structure (Peñuelas and Filella, 1998). Structural alterations modify reflection of light from plant leaves or canopies. These changes can be visualised by reflectance imaging in the visible light spectrum (400–700 nm) or near-IR spectrum (0.7–1.3 μm). In visible light spectrum, an image is a spatial 2D-light intensity function which can be described by:

$$f(x,y) = i(x,y)r(x,y) \tag{6}$$

$$0 < i(x,y) < \infty \tag{7}$$

$$0 < r(x,y) < 1 \tag{8}$$

where $i(x,y)$ is the illumination (amount of light incident on the scene of object being viewed) and $r(x,y)$ is the reflectance (amount of lighted reflected by the objects in the scene being viewed). The value of $r(x,y)$ can be described by the dichromatic reflection model (Shafer, 1985):

$$r(x,y) = L_{surf} + L_{body} \tag{9}$$

where L_{surf} is the surface reflection (light reflected at the material surface) and L_{body} is the light body reflection (light reflected from the material body). The body reflection provides the characteristic object colour (Klinker, 1993). Thus, the visible image of a plant is a description of its light reflection characteristics. Factors leading to a decrease in light absorption automatically increase reflection and vice versa. The pattern of light emission from plant leaves or canopy as depicted by the subtle changes in the colour or the surface structure of its images can be used to quantify its physiological changes. In this study, RGB ratios, given by Eqs. (10)–(12), and GLCM texture features shown in Table 1, were used to quantify plant colour and surface structure

Table 1 – GLCM textural features as defined by Haralick et al. (1973)

Feature	Formula	Description
Entropy	$-\sum_{j}^{M}\sum_{i}^{N} P[a,b]\log P[a,b]$	Measures the randomness of grey distribution
Energy	$\sum_{i}^{M}\sum_{j}^{N} P^2[a,b]$	Measures the number of repeated pairs
Contrast	$\sum_{i}^{M}\sum_{j}^{N}(a-b)^2 P[a,b]$	Measures the local contrast of an image
Correlation	$\sum_{i}^{M}\sum_{j}^{N}\frac{(a-\mu)(b-\mu)P[a,b]}{\sigma^2}$	Provides the correlation between two pixels in a pair
Homogeneity	$\sum_{i}^{M}\sum_{j}^{N}\frac{1}{1+(a-b)^2} P[a,b]$	Measures local homogeneity of a pixel pair

Notation: $P[a,b]$ is the (a,b)th element of a normalised co-occurrence matrix; μ and σ are the mean and standard deviation of the pixel elements given by the following relations:

$$P(a,b) = \frac{N(a,b)}{M}$$

$$\mu = \sum_{i}^{M} a \sum_{j}^{N} P[a,b]$$

$$\sigma = \sum_{i}^{M}(a-\mu)^2 \sum_{j}^{N} P[a,b]$$

where $N(a,b)$ = number of counts in the image with pixel intensity a followed by pixel intensity b at one pixel displacement to the left and M is the total number of pixels.

changes, respectively,

$$r = \frac{R}{R+G+B} \quad (10)$$

$$g = \frac{G}{R+G+B} \quad (11)$$

$$b = \frac{B}{R+G+B} \quad (12)$$

where r, g and b are the red, green and blue ratios, respectively, and R, G and B are the pixel intensities of the red, green and blue band widths, respectively.

2.2. Sunagoke moss sample

Fig. 1 shows the Sunagoke moss sample used in this study. The sample was grown on glass wool media in a rectangular glass dish of dimensions, $150 \times 100 \times 20$ mm. It was subjected to different water states as a means of manipulating its physiological status. Water state is defined here as the amount of water available to the sample at the beginning of each day of data acquisition in grams of water per gram of sample initial dry weight. Water content and water state are used interchangeably in this paper. Six water states were considered, i.e. 5, 4, 3, 1.5, 0.5 and 0 g g^{-1}. No nutrition was provided to the sample. It is worth noting here that preliminary experiments have shown that Sunagoke moss can absorb up to eight times its own weight of water.

Fig. 1 – Sunagoke moss sample used in this study.

2.3. Experimental data acquisition system

The set-up of the data acquisition system used in the study is shown in Fig. 2. It comprised of an imager (ii-1064, Horiba Ltd., Japan), with IR and RGB image sensors, mounted on a stand to view the sample at approximately 90°. The IR sensor comprised of a 64-element thermopile array arranged in an 8×8 matrix of 0.5 mm^{-2}. It output single temperature readings in °C (resolution = ±0.1 °C/1 °C) averaged over its instantaneous field of view (IFOV). Its precision was ±2 °C for the conditions of this experiment. The visible light imager comprised a CMOS colour image sensor and had a resolution of 320×240 pixels. The distance between the imager and the sample was 270 mm giving an IFOV of 12×12 mm^2 for the IR image sensor. Ignoring parallax effects, the field of view (FOV) was the same for both sensors. A reference emitter was made from a standard black tape, whose emissivity was 0.95 (Horiba, Japan), and located level with the surface of the sample within the FOV of both sensors. A background radiation mirror made of an aluminium foil was fitted directly in front of the sample when it was deployed. Thermistors (203AT), with a measurement accuracy of ±0.3 (−20 to 80 °C), connected to digital data loggers (Thermo recorder, TR-71U, T&D Corp., Japan), were used to measure the direct contact temperature of the reference emitter and the ambient conditions of the growth chamber. The experiment was conducted in a growth chamber (Biotron NC 350, NK-system, Japan) under conditions of 15 °C, temperature, 60%, relative humidity and 12-h light and dark periods. The average light intensity inside the growth chamber (measured by Li-250A-light meter; Li-COR, USA) was 86.54 μmol s^{-1} m^{-2} or 7.21 Klux (400–700 nm). All data were processed using a laptop computer (Toshiba Satellite; Toshiba, Japan).

2.4. Determination of the surface emittance of Sunagoke moss

The first part of the study involved determination of the surface emittance of the sample. With the background mirror

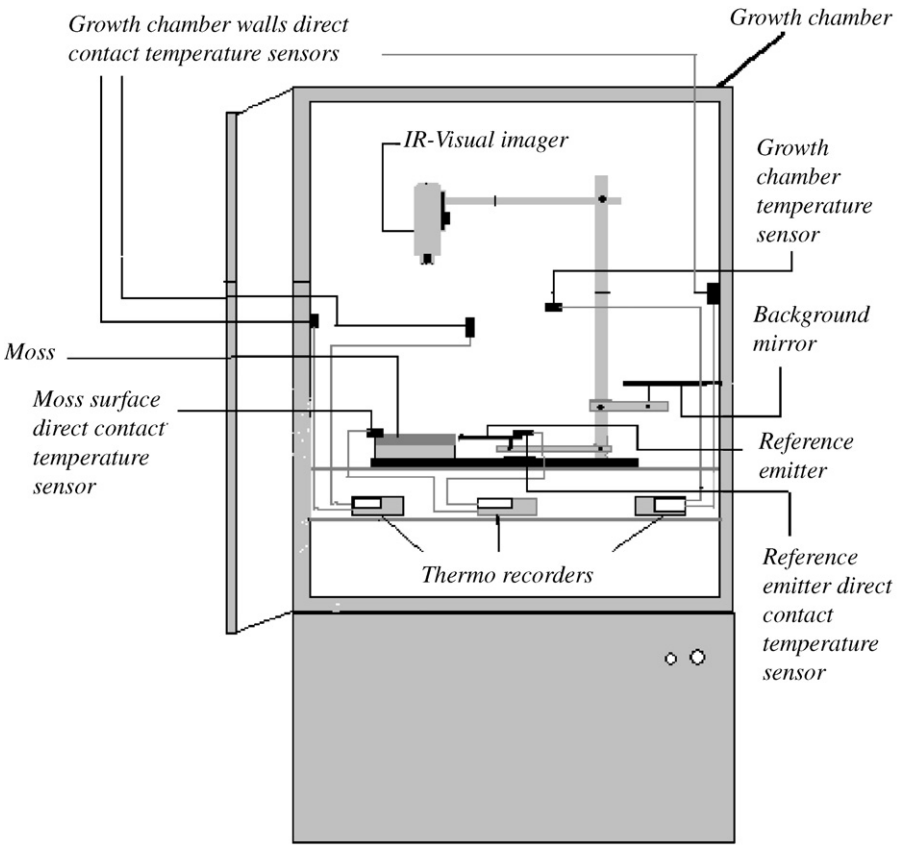

Fig. 2 – Experimental set-up of the thermal-reflectance imaging system used in the study.

deployed and the emissivity of the IR sensor set to 1, thermal data were acquired at 15-min intervals for 24 h. Meanwhile, five times its own dry weight of water was applied to the sample which remained in the growth chamber for 1 day. On the second day, the background mirror was removed and thermal data from the sample and the reference emitter were acquired at 15-min intervals over 6 days. At the start of each day the water state of the sample was computed and replenished to reach the target for the day. Using the thermal data obtained, the emittance of the sample was determined by

$$e_{ms} = \frac{(T^4_{e=1,ms} - T^4_{back})}{(T^4_{e=1,ref} - T^4_{back})} e_{ref} \tag{13}$$

where e_{ms} is the emissivity of the moss surface, $T_{e=1,ms}$ and $T_{e=1,ref}$ are the equivalent black body moss surface and reference emitter IR temperatures, respectively, T_{back} is the background temperature measured by the background mirror and e_{ref} is the emissivity of the reference emitter.

2.5. *Determination of the crop water stress index*

Five times its own initial dry weight of water was applied to the sample and it was allowed to acclimatise in the growth chamber for 1 day. Thermal and visible light images of the sample and reference emitter were then simultaneously acquired every 15 min for 6 days. At the start of each day, the water state of the sample was determined and replenished to reach the target for the day. The emissivity of the thermal imager was kept at 1. Thermo recorders were set to record the temperature simultaneously with image acquisition. Using thermal data obtained at each IFOV, apparent temperatures of the sample and reference emitter were computed by Eqs. (14) and (15), respectively:

$$T_{IR,ms} = \left(\frac{T^4_{e=1,ms} - (1 - e_{ms}) T^4_{back}}{e_{ms}} \right)^{1/4} \tag{14}$$

$$T_{IR,ref} = \left(\frac{T^4_{e=1,ref} - (1 - e_{ref}) T^4_{back}}{e_{ref}} \right)^{1/4} \tag{15}$$

where $T_{IR,ms}$ and $T_{IR,ref}$ are the apparent IR surface temperatures of the sample and the reference emitter, respectively. Each value obtained by Eq. (14) was corrected using Eq. (15) to obtain the final temperature values:

$$T_{F,ms} = T_{IR,ms} - (T_{IR,ref} - T_{DC,ref}) \tag{16}$$

where $T_{F,ms}$ is the final temperature of the sample in °C and $T_{DC,ref}$ is the direct contact temperature of the reference emitter in °C. The daily average temperature values obtained by Eq. (16) and the daily average ambient temperature inside the growth chamber were used to calculate the daily CWSI using Eq. (5).

2.6. Determination of RGB ratios and textural features

Visual images of the sample were processed using ImageJ software (National Institute of Health (NIH), USA) to give daily average *r*, *g* and *b* ratios and GLCM textural features. Prior to determination of these features, the images were pre-processed by selecting a region of interest (ROI), cropping, resizing to 120×96 pixels and carrying out histogram equalisation. The ROI was selected as the area of the image lying within the canopy of the sample. ROI sub images were created by cropping and resizing and then arranged into stacks for faster analysis. To improve contrast, histogram equalisation was performed to redistribute image pixel intensities. The RGB ratios were computed using Eqs. (9)–(11). The textural features were determined using the relations shown in Table 1.

2.7. Error analysis

Thermal data obtained in this study were subject to random errors, compensation for emittance and background radiation errors, FOV systematic errors and direct contact temperature measurement errors. The basic level of random error was described by:

$$\sigma_p = \sqrt{\frac{1}{N}\sum_{p=1}^{N}(T_p - T_m)^2} \tag{17}$$

where σ_p is the standard deviation, T_p is the temperature data point, T_m is the spatial mean of all temperatures and N is the number of temperature data points evaluated. Because of random errors, the uncertainty of individual temperature data depends on the number of frames averaged over time. The average basic random errors computed for every four frames were averaged over 1 h, and Eq. (18) was used to calculate the corresponding uncertainty:

$$\delta T_{p,ran} = \frac{\sigma p}{\sqrt{n}}(mn - a) \tag{18}$$

where $\delta T_{p,ran}$ is the random error uncertainty, n is the number of hours over which frames are averaged and m and a are, respectively, the gradient and intercept of a linear regression of the ratio between the determined standard deviation and the expected standard deviation (assuming the errors follow a normal distribution). The uncertainties of the apparent thermal data of reference emitter, $\delta T_{IR,ref}$, and the apparent IR temperature of the sample, $\delta T_{IR,ms}$, were evaluated using the same procedure. Uncertainties of the ambient direct contact temperature,δT_A, and the reference emitter direct contact temperature, $\delta T_{DC,ref}$, were estimated using Eq. (17). The most probable total uncertainty, δT, of the thermal data was then estimated by:

$$\delta T = \sqrt{\delta^2 T_{IR,ms} + \delta^2 T_{IR,ref} + \delta^2 T_{DC,ref} + \delta^2 T_A} \tag{19}$$

A copper plate of dimensions $3 \times 200 \times 300$ mm was used to evaluate the uncertainty arising from the performance of the IR thermal imager across its FOV, δT_{FOV}. Because the plate was kept overnight in the growth chamber, it was assumed to be isothermal. Twenty-one images of the plate were acquired over the entire FOV of the imager. Every thermal data point on the plate was then evaluated for deviation from the mean of all temperatures within each frame and δT_{FOV} was determined using the procedure outlined above.

The visible light image data were also subject to errors stemming from the level of noise in the imaging system, image acquisition, pre-processing, and the feature extraction processes. The uncertainty arising from these errors was estimated from the average standard deviations of grey levels of the RGB channels in the sample images.

3. Results

3.1. Accuracy of measurements

Table 2 summarises the range of different errors for the thermal data obtained in the study. The results show that the thermal data acquired during the dark period generally had a higher uncertainty than that acquired during the light period. The results in Table 3 show that the maximum total uncertainty of the IR-measured temperature was $\pm 0.5\,^{\circ}C$, compared to a theoretical value of $\pm 2.0\,^{\circ}C$ for the IR sensor. The maximum uncertainty of the visible light data was ± 7.65

Table 2 – Range of uncertainties for temperature data obtained in the study

Uncertainty	Ranges in °C		
	Light period	Dark period	24-h period
$\delta T_{IR,ms}$	0.14–0.45	0.18–0.78	0.16–0.70
$\delta T_{IR,ref}$	0.09–0.14	0.15–0.28	0.33–0.57
$\delta T_{DC,ref}$	0.10–0.19	0.12–0.22	0.24–0.67
δT_A	0.11–0.23	0.09–0.20	0.10–0.32

Notation: $\delta T_{IR,ms}$ = uncertainty of each of the sample's apparent temperature datum; $\delta T_{IR,ref}$ = uncertainty of each reference emitter's apparent temperature datum; $\delta T_{DC,ref}$ = uncertainty of reference emitter's directly measured temperature; and δT_A = uncertainty of each ambient temperature datum.

Table 3 – Uncertainty of thermal and visible light imaging data for Sunagoke moss sample

Day	Maximum possible uncertainty			
	Thermal data (°C)	Visible light data in grey levels		
		R	G	B
1	0.37	7.65	7.34	6.48
2	0.32	7.25	7.13	7.33
3	0.29	6.22	5.77	7.19
4	0.37	6.54	6.91	7.27
5	0.30	4.97	5.13	4.89
6	0.50	4.77	5.04	5.18

pixel intensity level attributed to the red channel of the RGB images.

3.2. *Surface emissivity of Sunagoke moss*

From Table 4 the surface emissivity of the sample, e_{ms}, ranged between 0.79 and 1.0 at 0 and 5.0 g g^{-1} water contents, respectively. An average value of 0.93 was used for all temperature calculations. The results show that the emissivity of the sample generally increased with the water content but remained constant at water contents between 1.5 and 3.0 g g^{-1}.

3.3. *Change of the crop water stress index (CWSI) with time*

The daily average values of the water content of the sample, its surface temperature, and its CWSI are also shown in Table 4. The surface temperature and CWSI increased inversely with water content. Fig. 3 shows the hourly variation, surface temperature and CWSI of the sample for the last three days of the experiment. No significant changes in these parameters were observed during the first 3 days of the experiment. The CWSI generally increased with surface temperature. However, there were some deviations attributed to variations in the physiological changes of the sample during the light and dark periods. The ambient temperature of the growth chamber remained fairly constant during the experiment.

Table 4 – Average water content, surface temperature and crop water stress index of the sample

Day	Sunagoke moss water state (g g^{-1})	Surface temp. (°C)	Ambient temp. (°C)	Emissivity
1	5.0	12.41	17.58	0.79
2	4.0	12.40	17.51	0.87
3	3.0	12.39	17.45	0.96
4	1.5	12.42	17.57	0.97
5	0.5	15.49	17.35	0.97
6	0.1	17.32	17.61	1.00

3.4. *Variation of canopy CWSI, colour and texture with water status*

Table 5 shows the daily average GLCM textural features and RGB colour ratios of the sample. All the textural features showed a critical point on the third day. This was a maximum for energy, correlation and homogeneity, and a minimum for inertia and entropy. The features showed minimal change between the 3rd and the 4th day. Energy, correlation and homogeneity showed a decrease after the 4th day while inertia and entropy increased. Similarly, all colour ratios showed a critical point on the 3rd day. Ratios *r* and *g* increased up to the 3rd day after which they decreased. This was reversed for the *b* ratio.

Fig. 4a shows that ratios *r* and *g* increased with the water content up to 1.5 g g^{-1}, remained fairly constant between 1.5 and 3.0 g g^{-1} after which the ratios decreased. This was reversed for the *b* ratio. CWSI generally varied inversely with the water content. A linear regression between the CWSI and water content gave a coefficient of determination, $R^2 = 0.85$. Regressing the data as a quadratic polynomial gave $R^2 = 0.99$. Thus, there was a high correlation between CWSI and water content in the sample. Fig. 4b shows that the energy feature increased with the water content up to 1.5 g g^{-1} but decreased after 3.0 g g^{-1}. This was reversed for entropy. It

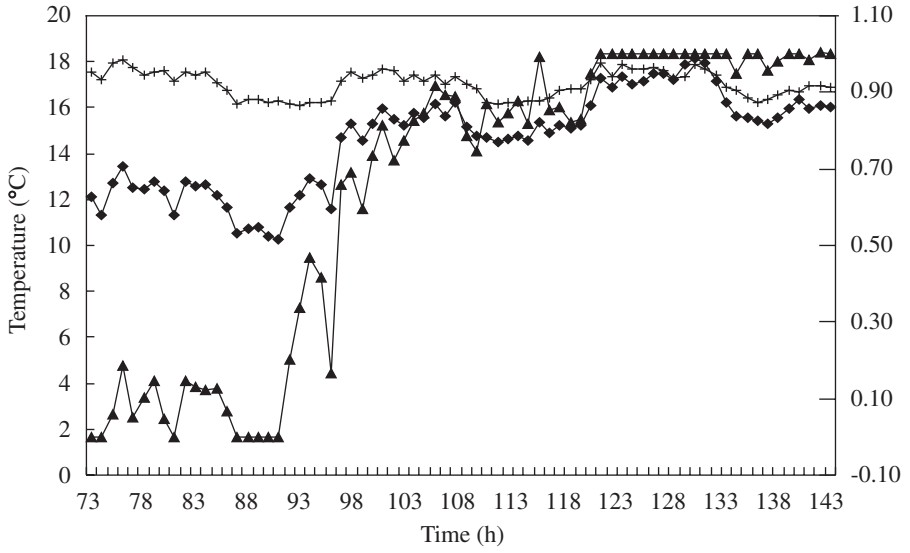

Fig. 3 – Hourly variation of Sunagoke moss sample surface temperature, growth chamber ambient temperature and sample's crop water stress index (CWSI) for the 3rd, 4th and 5th days. +–+, Growth chamber ambient; ◆–◆, sunagoke moss sample; ▲–▲, crop water stress index.

Table 5 – Sunagoke moss sample surface daily average textural features and RGB grey-level ratios

Day	Average textural features					Average RGB ratios		
	Energy	Inertia	Correlation	Homogeneity	Entropy	*r*	*g*	*b*
1	0.000146	878	0.000443	0.0535	9.12	0.35	0.34	0.31
2	0.000137	835	0.000454	0.0529	9.13	0.35	0.34	0.31
3	0.000151	714	0.000531	0.0579	9.03	0.38	0.38	0.24
4	0.000154	759	0.000530	0.0560	9.01	0.39	0.39	0.22
5	0.000123	1930	0.000246	0.0358	9.32	0.37	0.34	0.29
6	0.000125	1890	0.000260	0.0358	9.30	0.37	0.34	0.29

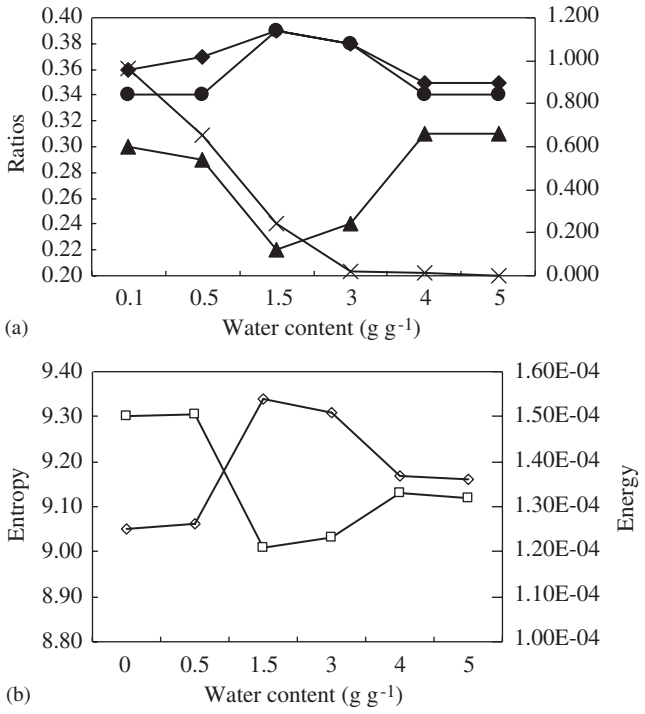

Fig. 4 – Variation of infrared thermal and visible light imaging features with water content in Sunagoke moss: (a) crop water stress index (CWSI) and RGB ratios (b) texture features: ◆–◆, *r* ratio; ■–■, *g* ratio; ▲–▲, *b* ratio; ×–×, CWSI; ◇–◇, energy; □–□, entropy.

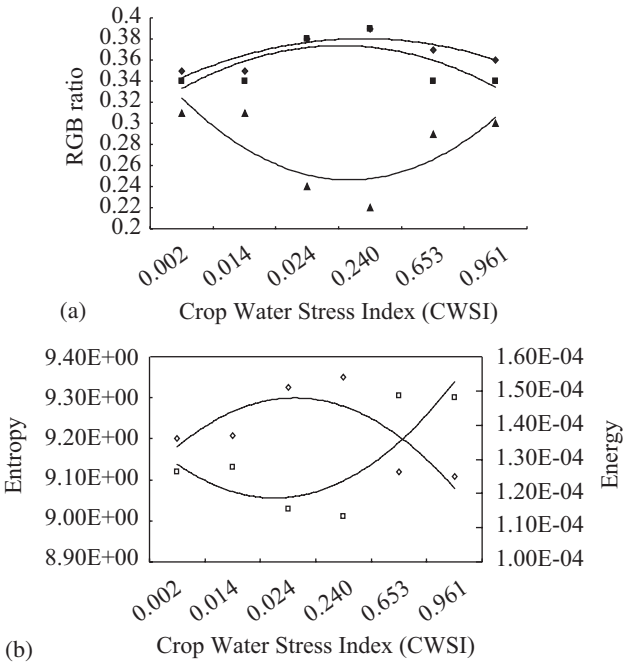

Fig. 5 – Visible light imaging features of Sunagoke moss sample as quadratic polynomial functions of crop water stress index (CWSI): (a) RGB colour ratios; (b) texture features. ◆–◆, *r* ratio, $y = -0.0045x^2+0.0278x+0.337$, $R^2 = 0.71$; ■–■, *g* ratio, $y = -0.0064x^2+0.047x+0.296$, $R^2 = 0.56$; ▲–▲, *b* ratio, $y = 0.0109x^2-0.0725x+0.367$, $R^2 = 0.62$; ◇–◇, energy, $y = -3E-06x^2-2E-05x+0.0001$, $R^2 = 0.65$; □–□, entropy, $y = 0.269x^2-0.148x+0.9.2595$, $R^2 = 0.67$.

can therefore be deduced that the sample exhibited some water-related stress at water contents below 1.5 g g^{-1} and above 3.0 g g^{-1}.

3.5. *Correlation between colour and texture features and CWSI*

Fig. 5 shows RGB ratios and texture features as quadratic polynomial functions of CWSI for the sample used in this study. The coefficient of determination, R^2, of *r*, *g* and *b* was 0.71, 0.56 and 0.62, respectively, and 0.67 and 0.65 for energy and entropy, respectively. Thus, there was a significant correlation between the colour and texture of the sample and its CWSI.

4. Discussion

The main assumption underlying this study was that changes in the canopy transpiration patterns, reflectance and surface structure of a plant are external manifestations of its internal physiological states. Visible light imaging was used to report changes in the surface structure and reflectance and IR thermal imaging was used to report changes in transpiration patterns in the Sunagoke moss sample. CWSI was used to quantify changes in its transpiration patterns. The texture features given in Table 1 were used to depict changes in the sample surface structure while the colour

ratios determined by Eqs. (10)–(12) were used to depict changes in its reflectance.

The results in Table 4 and Figs. 3 and 4 show that CWSI is a good indicator of drought water stress in Suagoke moss. This agrees with a number of studies (González-Dugo et al., 2006; Jackson, 1982; Jackson et al., 1981; Wanjura and Upchurch, 2000) and is in line with the expected biophysical behaviour of plants. As the water content decreases, transpiration cooling of the surface of a plant decreases leading to an increased surface temperature which consequently increases the CWSI. The significant correlation between the colour ratios and texture of the sample and its CWSI in Fig. 5 implies that these features can also be used to detect water stress in the plant. The results in Table 5 show that the sample was under some water-related physiological stress between the 1st and the 3rd day and between the 4th and the 6th day of the experiment. However, the effects of such stress were minimal between the 3rd and the 4th day which corresponded to 3.0 and 1.5 $g\,g^{-1}$ water contents, respectively. From Fig. 4 it can be deduced that CWSI is only effective in detecting drought water stress in Sunagoke moss. However, texture and colour can be good biophysical indicators of both excess and deficit water stress-related physiological changes in the plant.

Thus, simultaneous changes in colour, texture and temperature in Sunagoke moss canopy are direct indicators of its physiological state. Sunagoke moss is highly resilient and exhibits a high level of desiccation tolerance (i.e. the ability to function while dehydrated). This is a desirable quality for a biological roof greening material as it ensures the aesthetic soundness of the roof even when the material is dry. The results in Table 5 and Fig. 4 show that this quality does not affect the correlation between the water content of the sample and its colour and texture. It can be generally deduced that the sample was 'relaxed' biophysically, at water states between 1.5 and 3.0 $g\,g^{-1}$. This implies that the optimum amount of water to apply to Sunagoke moss is 1.5–3.0 times its dry weight. This will cause the plant to experience insignificant water-related stress and optimise water utilisation.

4.1. *Uncertainty of the results*

Canopy temperature is affected by the surface emittance of the plant, ambient temperature, background thermal radiation and humidity. Consequently, three factors introduce error into measurement of plant surface temperature by IR thermal imaging: the incorrect determination of plant emissivity and background radiation, the inaccuracy of the imager itself and its basic system noise including optics, scanning, electronics, and the emission and detection of IR radiation. The error caused by the incorrect estimation of the emissivity and background radiation varies with the wavelength utilised by the imager but is similar for all thermal imagers. The emissivity of the sample used in this study varied between 0.78 and 1.0 for 0 $g\,g^{-1}$ and 5.0 $g\,g^{-1}$ water contents, respectively. An average emissivity of 0.93 was used for temperature calculations. The uncertainty for this average value was ± 0.06. However, this uncertainty is negligible due to averaging of the thermal data across many spatial and time frames. Furthermore, plants, as with other biological systems, are characterised by many natural dynamics and non-linearity and some uncertainty in their emissivity is likely.

The maximum possible uncertainty of each temperature datum within the FOV (δT_{FOV}) of the thermal imager was $\pm 1.06\,^{\circ}C$ against $\pm 2.0\,^{\circ}C$ quoted for the IR sensor for the conditions of the experiment. Thus, by averaging the thermal data across many time frames, the accuracy of the imager was improved by about 50%. However, the maximum standard deviation of the temperature data within the FOV of the imager was 4.31 °C. This was attributed to errors introduced by the use of a copper plate to evaluate this value. Although it was assumed to be isothermal, the thickness of the plate was only 3 mm and there was no system to ensure that it was uniformly cooled. However, the standard deviation of 86% data points falling within the FOV of the imager was less than 2.0 °C. The third source of error was random noise from various sources in thermal image and thermal data analysis. The accuracy of thermal data depends on the characteristics of the imaging system and the techniques used to record and process the thermographic data. The results in Table 2 suggest that the thermal data of the sample had a higher uncertainty in the dark period than in the light period. This could possibly be attributed to some net heat from the light source in the growth chamber. The maximum possible total uncertainty for the IR-measured thermal data for the sample was $\pm 0.50\,^{\circ}C$. However, the value of uncertainty was very low considering the controls used and the number of multiple frames averaged.

Errors stemming from imaging system noise level, image acquisition, pre-processing and the feature extraction processes affected the certainty of the visible light imaging data. However, errors attributed to image acquisition and imager optics noise were assumed to form the bulk of the uncertainty of the visible light image data used in the study. The ii-1064 imager was capable of both IR thermal and visible light imaging. Thus, its efficiency was divided between these two imaging modes. This affected the clarity with which the RGB images were acquired. The inherent optics noise also contributed to the acquisition errors. Maintaining controlled conditions in the growth chamber involved spraying of atomised water at regular intervals. This reduced the light intensity in the chamber and impaired the optical lens of the imaging sensor from time to time and caused some error in image acquisition. The uncertainty arising from these errors was estimated by average standard deviations of grey levels of the RGB channels. This was found to be a maximum of ± 7.65 pixel intensity and attributed to red channel.

5. Conclusions

In this study, CWSI, RGB colour ratios and GLCM texture were used to detect water stress in a Sunagoke moss sample. The results showed a clear correlation between the CWSI, RGB colour ratios and GLCM textural features of the sample and its water content. The sample was found to exhibit water-related physiological stress at water contents below 1.5 $g\,g^{-1}$ and above 3.0 $g\,g^{-1}$ (grams of water per gram of dry Sunagoke moss) but appeared to be "relaxed" physiologically at water contents in between.

The maximum possible total uncertainty of thermal data acquired in the study was $\pm 0.50\,^{\circ}C$ at $17\,^{\circ}C$, ambient temperature. The maximum uncertainty of the visible light data was ± 7.65, pixel intensity and attributed to red bandwidth. Thermal imaging could only detect drought water stress while visible reflectance imaging was able to detect both drought and flood water stress in the sample. It is concluded that a combination of thermal and visible light imaging as espoused in the TRIS systems can be used to detect both deficit and excess water stress in Sunagoke moss. Although only Sunagoke moss was used in this study, the TRIS system is novel and could be extended to other biotic and abiotic stress detection in other plants. As for the results with Sunagoke moss, from this study, we deduce that the optimum amount of water to ensure its best aesthetic and physiological states and optimum water utilisation is in the range of 1.5–3.0 times its dry weight. However, more studies incorporating photosynthesis measurements need to be carried out to verify this and to develop thermal-reflectance digital fingerprints for water stress before a prototype of TRIS systems can be fully tested.

REFERENCES

Al-Fara A; Meyer G E; Schade G R; Horst G L (2000). Dynamic analysis of moisture stress in tall Fescue (*Festuca arundinacea*) using canopy temperature, irradiation and vapour deficit. Transactions of ASAE, **43**(1), 101–109

Aro E M; Niemi H; Valanne N (1981). Structural and functional studies on bryophyte photonsythesis. In: Photonsythesis (Akoyunoglou G, ed), Vol. 3, pp 327–335. Balaban Int. Sci. Serv., Philadelphia, PA

Bowen E J (1933). The mechanism of water conduction in Musci considered in relation to habitat. II. Mosses growing in dry environments. Annals of Botany (London), **47,** 889–912

Chaerle L; Van Der Straeten D (2001). Seeing is believing: imaging techniques to monitor plant health. Biochimica et Biophysica Acta, **1519,** 153–166

Clarke T R (1997). An empirical approach for detecting crop water stress using multispectral airborne sensors. Horticulture Technology, **7**(1), 9–16

Foucher P; Revollo P; Vigouroux B; Chassériaux G (2004). Mophological image analysis for the detection of water stress in potted Forsythia. Biosystems Engineering, **89**(2), 131–138

González-Dugo M P; Moran M S; Mateos L; Bryant R (2006). Canopy temperature variability as an indicator of crop water stress severity. Irrigation Science, **24**(4), 233–240

Hall S G; Lima M (2001). Problem-solving approaches and philosophies in biological engineering: challenges from technical, social, and ethical arenas. Transactions of ASAE, **44**(4), 1037–1041

Haralick R M; Shanmugan K; Dinstein I (1973). Textural features for image classification. IEEE Transactions on Systems, man and Cybernetics SMC, **3,** 610–621

Hashimoto Y; Ino T; Kramer J P; Naylor W Aubrey; Strain R B (1984). Dynamic analysis of water stress of sunflower leaves by means of thermal image processing. Plant Physiology, **76,** 266–269

Jackson R D (1982). Canopy temperature and crop water stress. In: Advances in Irrigation (Hellel D I, ed), Vol. 1, pp 43–85. Academic Press

Jackson R D; Idso S B; Reginato R J; Penter Jr P J (1981). Canopy temperature as a crop water stress indicator. Water Resources Research, **17**(4), 1133–1138

Jensen M E; Burman R D; Allen R G eds (1990). Evapotranspiration and irrigation water requirements. ASAE Manuals and Reports on Engineering Practice No. 7, ASCE, 345 E. 47th S, NY

Kacira M; Ling P P; Short T H (2002a). Establishing crop water stress index (CWSI) threshold values for early, non-contact detection of plant water stress. Transaction of ASAE, **45**(3), 775–780 ISSN:0001-2351

Kacira M; Ling P P; Short T H (2002b). Machine vision extracted plant movement for early detection of plant water stress. Transaction of ASAE, **45**(4), 1147–1153

Klinker G (1993). A Physical Approach to Color Image Understanding. A K Peters, Ltd., Wellesley, MA

Ondimu S; Murase H (2006). Thermal properties of living roof greening material by inverse modeling. Applied Engineering Agriculture, **22**(3), 435–441

Peñuelas J; Filella I (1998). Visible and near-infrared reflectance techniques for diagnosing plant physiological status. Trends in Plant Science, **3,** 151–156

Pieters C A (1975). Thermography and plant physiology. Bibliotheca Radiology, **6,** 210–217

Sena Jr D G; Pinto F A C; Queiroz D M; Viana P A (2003). Fall armyworm damaged maize plant identification using digital images. Biosystems Engineering, **85**(4), 449–454

Shafer S A (1985). Using color to separate reflection components. Color Research and Application, **10**(4), 210–218

Taiz L; Zeiger E (2002). Plant Physiology. Sinauer Associates Inc., Sunderland, MA, USA

Ushada M; Murase H (2006). Identification of a moss growth system using an artificial neural network model. Biosystems Engineering, **94**(2), 179–189

Valanne N (1984). Photonsythesis and photonsythetic products in mosses. In: The Experimental Biology of Bryophytes (Dyer A J; Duckett J G, eds), pp 257–273. Academic press, London

Wanjura D F; Upchurch D R (2000). Canopy temperature characterizations of corn and cotton water status. Transactions of ASAE, **43**(4), 867–875

Zandonadi R S; Pinto F A C; Sena Jr D G; Queiroz D M; Viana P A; Mantovani E C (2005). Identification of lesser cornstalk borer-attacked maize plants using infrared images. Biosystems Engineering, **91**(4), 433–439